
Multi-granular body modeling with Redundancy-Free Spatiotemporal Fusion for Text-Driven Motion Generation

Xingzu Zhan¹ Chen Xie¹ Honghang Chen¹ Haoran Sun¹ Xiaochun Mai^{1*}

¹ Shenzhen University, Shenzhen, China

xiaochunmai@163.com

Abstract

Text-to-motion generation is a rapidly growing field at the nexus of multimodal learning and computer graphics, promising flexible and cost-effective applications in gaming, animation, robotics, and virtual reality. Existing approaches often rely on simple spatiotemporal stacking, which introduces feature redundancy, while subtle joint-level details remain overlooked from a spatial perspective. To this end, we propose a novel HiSTF Mamba framework composed of three key modules: *Dual-Spatial Mamba*, *Bi-Temporal Mamba*, and the *Dynamic Spatiotemporal Fusion Module* (DSFM). Dual-Spatial Mamba incorporates “part-based + whole-based” parallel modeling to capture both whole-body coordination and fine-grained joint dynamics. Bi-Temporal Mamba employs a bidirectional scanning strategy that effectively encodes short-term motion details and long-term dependencies. DSFM further removes redundancy and extracts complementary information from temporal features, then fuses them with spatial features, yielding an expressive spatio-temporal representation. Experimental results on the HumanML3D dataset demonstrate that HiSTF Mamba achieves robust performance across multiple evaluation metrics; These findings validate the effectiveness of HiSTF Mamba in achieving high fidelity and strong semantic alignment in text-to-motion generation.

1 Introduction

Text-to-motion aims to generate human motion sequences based on natural language descriptions, and has emerged as a key research direction at the intersection of multimodal learning and computer graphics. Using textual input to drive human motion generation, text-to-motion provides a flexible and cost-effective approach for applications such as games [1], animation [2], robotic interaction [3], and virtual reality (VR).

Early motion generation has predominantly relied on two mainstream paradigms: Generative Adversarial Networks (GANs) [4] and Variational Autoencoders (VAEs) [5]. GAN-based approaches [6–10] leverage adversarial training to produce diverse motion sequences but suffer from mode collapse, leading to observable distortions in limb movement amplitudes [11]. Meanwhile, VAE-based models [12–15] utilize latent-space representations to maintain temporal continuity; however, they often sacrifice motion details due to insufficient feature disentanglement. Although hybrid architectures [16] attempt to jointly capture spatio-temporal features, parameter redundancy and inadequate cross-dimensional interactions still limit their performance. In recent years, diffusion-based motion generation methods [17] have emerged rapidly. They employ a progressive generation mechanism grounded in probabilistic denoising to strike a balance between diversity and realism, thereby circumventing many inherent drawbacks of conventional GANs and VAEs. For example, MDM [18],

*Corresponding author.

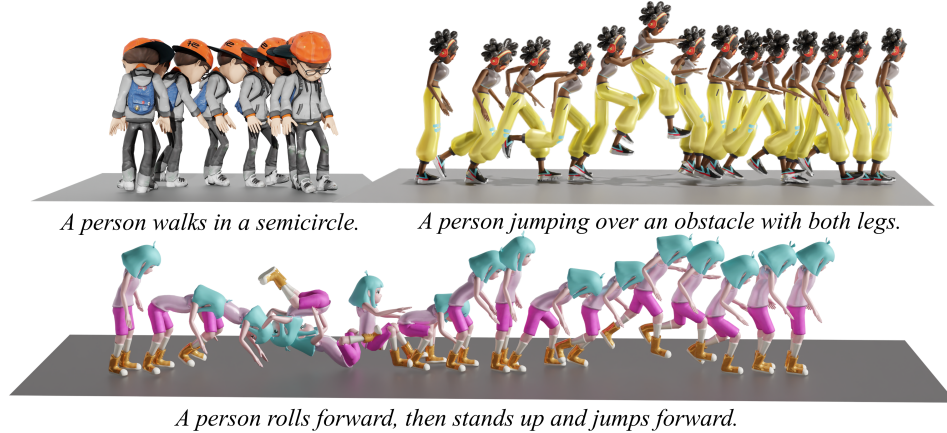


Figure 1: Qualitative visualization of HiSTF Mamba’s generated motions.

MLD [19], MotionDiffuse [20], and MoFusion [21] have shown notable advantages in visual fidelity, motion smoothness, and scalability. To further enhance spatiotemporal modeling, FineMoGen [22] and Spatio-Temporal Graph Diffusion [23] design separate temporal and spatial modules, then adopt serial or parallel strategies to capture richer dependencies. Motion Mamba [24] applies Mamba [25] to these modules, improving efficiency and reducing training time.

However, despite the promising progress in efficiency, Motion Mamba[24] still has significant limitations in modeling fine-grained joint details and effectively fusing spatio-temporal features. The reasons for these limitations are two-fold. (1) *Lacking the spatial modeling and feature learning of local body.* Although feeding the entire motion matrix into the network at the same time can capture the overall motion pattern, its fixed information capacity severely compresses early joint data as training progresses, thereby neglecting subtle relationships between individual joints or limbs. Furthermore, Selective State Space Models (Selective SSMs) typically discards these essential local details, pushing the model toward broad motion structures rather than subtle joint dynamics. (2) *Inadequate spatio-temporal fusion.* While Motion Mamba attempts to improve the fusion of spatio-temporal features by stacking spatio-temporal modules, this approach often leads to repeated extraction of similar or overlapping features, leaving subsequent layers with limited benefit from redundancy and inefficient learning. These redundancies significantly increase computational costs, forcing the model to spend resources on removing duplicate features rather than polishing critical spatio-temporal details, thus reducing the fidelity of motion generation.

To address these limitations in modeling fine-grained joint details and effectively fusing spatio-temporal features, we propose HiSTF Mamba. HiSTF Mamba consists of three key components: Dual-Spatial Mamba, Bi-Temporal Mamba, and DSFM. Concretely, Dual-Spatial Mamba adopts a parallel strategy “Part-based + Whole-based”, ensuring that the model can capture fine-grained joint details, while preserving coarse-grained whole-body coordination. Meanwhile, the Bi-Temporal Mamba block employs a bidirectional selected SSMs to scan the time dimension both forward and backward, capturing both short-term cues and long-term dependencies to ensure temporal coordination. Finally, rather than simply stacking spatiotemporal modules, we propose DSFM, which removes redundant temporal features from Bi-Temporal Mamba, extracts complementary information, and fuses it with the spatial output from Dual-Spatial Mamba for more efficient spatiotemporal fusion. Thus, HiSTF Mamba accommodates both global and local, long-range and short-range, as well as spatial and temporal dimensions, thereby significantly enhancing the fidelity and realism of text-to-motion generation. As evidenced by the visualizations in Fig 1, the synthesized motions not only closely align with the text descriptions but also exhibit full-body coordination and joint-level detail, reflecting the model’s effectiveness in capturing nuanced spatiotemporal patterns.

Overall, our contributions to the text-to-motion community can be summarized as follows:

1. In the Dual-Spatial Mamba block, we propose a “Part-based + Whole-based” parallel strategy that captures both whole-body coordination and fine-grained joint-level details, thereby improving the model’s ability to represent complex human body structures.

2. We design a Dynamic Spatiotemporal Fusion Module (DSFM) to perform redundancy removal and extraction of complementary information for temporal features, which is then fused with spatial features to construct a more efficient spatio-temporal representation. This significantly enhances the realism and smoothness of the generated motion sequences.
3. Extensive experiments on HumanML3D demonstrate that HiSTF Mamba achieves outstanding results across multiple metrics. Notably, it reduces the FID score from 0.281 to 0.189, a reduction of nearly 30%, while also achieving leading performance on other metrics. This validates HiSTF Mamba’s superiority in balancing high fidelity and strong text relevance.

2 Related Work

2.1 Text-to-Motion Generation

Early text-to-motion methods offered limited diversity: Text2Action [26] generated only upper-body motion, while JL2P [27] mapped text to poses one-to-one. Guo et al. [28] introduced a conditional VAE for variable-length outputs. TEMOS [29] employed a transformer-VAE for unified motion-text representations, and TEACH [30] extended this idea to longer sequences. MotionCLIP [31] aligned motion with CLIP [32], while TM2T [33] used VQ-VAE [34] to discretize motion into tokens. Although VQ-VAE-based methods [35–38] excel on FID, they risk information loss from quantization. Beyond GANs and VAEs, diffusion models [17] have proven adept at producing high-quality, diverse motions, exemplified by MotionDiffuse [20] and MDM [18]. MLD [19] moved diffusion to a latent space, and MotionLCM [39] added consistency distillation [40] for real-time generation. EMDM [41] further speeds sampling by reducing diffusion steps without degrading motion quality.

2.2 State Space Models

Transformers [42] excel in sequence modeling but often incur prohibitive quadratic complexity for high-resolution vision tasks. In response, State Space Models (SSMs)[43, 44] perform linear recurrences to capture long-range dependencies. For example, LSSL[44] employs continuous-time linear memory, while S4 [43], leveraging HiPPO [45] and FFT-based convolutions, significantly reduces computational overhead. Building on S4, Mamba [25] introduces dynamic gating and a parallel scan, accelerating inference without sacrificing global context. In vision tasks, SSM-based methods reduce Transformers’ computational cost by serializing images or videos into manageable sequences [25]. Vision Mamba [46] and VMamba [47] replace self-attention with scanning strategies, achieving Transformer-level performance. PlainMamba [48] and LocalMamba [49] use continuous or local scans to mitigate spatial discontinuities and improve segmentation. EfficientVMamba [50] further enhances efficiency with dilated convolutions and stride sampling, preserving accuracy under limited resources. Beyond scanning alone, additional modules can bolster local feature extraction: convolutional branches [51–53] are integrated into MambaIR [52] to merge convolutional and SSM layers for improved image restoration. Furthermore, SpikeMba [54] and VideoMamba [55] leverage SSMs for video generation and temporal modeling, efficiently handling lengthy sequences and reducing computational costs.

3 Method

In this section, we delineate the overall architecture and operational principles of the HiSTF Mamba, which aims to generate human motion guided by textual inputs. We begin by describing the theoretical foundations of Mamba [25], followed by an overview of the HiSTF Mamba. Finally, we detail the spatiotemporal modules: Dual-Spatial Mamba and Bi-Temporal Mamba, then proceed to discuss DSFM, which effectively fuses these spatiotemporal features.

3.1 Preliminaries

In S4 [43], under a discrete-time setting, a linear time-invariant (LTI) state space model is:

$$\begin{cases} h_t = A h_{t-1} + B x_t, \\ y_t = C h_t. \end{cases} \tag{1}$$

where $h_t \in \mathbb{R}^N$ is the hidden state, and $x_t, y_t \in \mathbb{R}$ are the input and output (extendable to multi-channel). The parameters A, B, C are trainable but, as an LTI system, cannot selectively emphasize or suppress specific inputs.

Selective SSMs [25] address this by making some key parameters vary dynamically with the input sequence, thus providing ‘‘content selectivity’’. Specifically, some parameters, such as B_t, C_t , and Δ_t , are determined by the current input x_t . Concretely:

$$\begin{cases} h_t = A(\Delta_t) h_{t-1} + B_t x_t, \\ y_t = C_t h_t, \end{cases} \quad \begin{cases} B_t = s_B(x_t), \\ C_t = s_C(x_t), \\ \Delta_t = \tau_\Delta(W_\Delta x_t). \end{cases} \quad (2)$$

By discretizing A, B into time-varying matrices $A(\Delta_t), B_t$, the system becomes *time-varying*, allowing it to filter out irrelevant information. This breaks LTI assumptions, preventing direct use of FFT-based global convolution. However, if $A(\Delta_t)$ is diagonal or similarly structured, a parallel scan on GPUs can achieve near $\mathcal{O}(L)$ complexity, and fusion or recomputation can reduce memory overhead.

3.2 HiSTF Mamba

To address the lack of local body structure modeling and suboptimal spatiotemporal fusion in text-to-motion generation, we propose **HiSTF Mamba**, a hierarchical spatiotemporal fusion approach, as illustrated in Fig. 2. Through three specialized components: N Bi-Temporal Mamba blocks, a Dual-Spatial Mamba block, and a DSFM module, HiSTF Mamba effectively captures fine-grained joint details and fuses spatiotemporal features. Specifically, the input sequence is first processed by N layers of Bi-Temporal Mamba to model rich temporal dependencies, and the resulting features are then fed into the Dual-Spatial Mamba block. Within this block, 2D dynamic convolution and Part SSMs extract joint-detail features from six body segments, which are then combined with the Whole SSMs’ global coordination to obtain the spatial feature S . Next, the N temporal features $\{T_1, \dots, T_N\}$ are passed to the DSFM for redundancy removal and subsequently fused with S , yielding a spatiotemporal motion representation that preserves both joint-level detail and overall body coordination.

In the sampling stage, we first encode the text condition with the CLIP [32] text encoder, apply random masking, and project it into the latent space. Meanwhile, we project the noise step T through an MLP and add it to the encoded text condition, obtaining $x^{(N+1)}$. we incorporate the $x^{(N+1)}$ with the motion sequence subjected to T steps of noise, yielding $\{x_T^1, x_T^2, \dots, x_T^N\}$, which is fed into the model to predict the clean sequence $\{\hat{x}_0^1, \hat{x}_0^2, \dots, \hat{x}_0^N\}$. The diffusion process then generates x^{T-1} from $\{\hat{x}_0^1, \hat{x}_0^2, \dots, \hat{x}_0^N\}$. Repeating this procedure T times ultimately produces a clean sequence $\{x_0^1, x_0^2, \dots, x_0^N\}$ that conforms to the text condition. This design balances global motion patterns with fine-grained joint dynamics, producing more accurate reconstructions. DPM-Solver++ [56] is used to accelerate sampling.

3.3 Bi-Temporal Mamba and Dual-Spatial Mamba

As shown in Figure 2, Bi-Temporal Mamba employs a bidirectional scanning mechanism to capture the contextual information of motion sequences in both forward and backward directions, thereby generating more coordinated and coherent motion sequences. Dual-Spatial Mamba adopts parallel Part-based and Whole-based learning, effectively capturing motion features that exhibit both fine-grained joint details and whole-body coordination.

Bi-Temporal Mamba. To generate coherent and smooth motion sequences, we employ Selected SSMs featuring a bidirectional scanning mechanism. We begin with an input sequence $T_{l-1} \in \mathbb{R}^{(B \times T \times D)}$, where B is the batch size, T is the sequence length, and D is the feature dimension. First, T_{l-1} is normalized and subsequently projected by a linear layer into a new representation space $\mathbb{R}^{(B \times T \times E)}$, yielding two transformed sequences X and Z . We then perform forward and backward scans over X , each governed by learnable parameters Δ, B , and C , which dynamically adjust the state update equation following Equation (2)

The forward and backward outputs are then elementwise multiplied with the nonlinear activation $\text{SiLU}(Z)$ and fused. Finally, a linear projection maps the fused representation back to the original

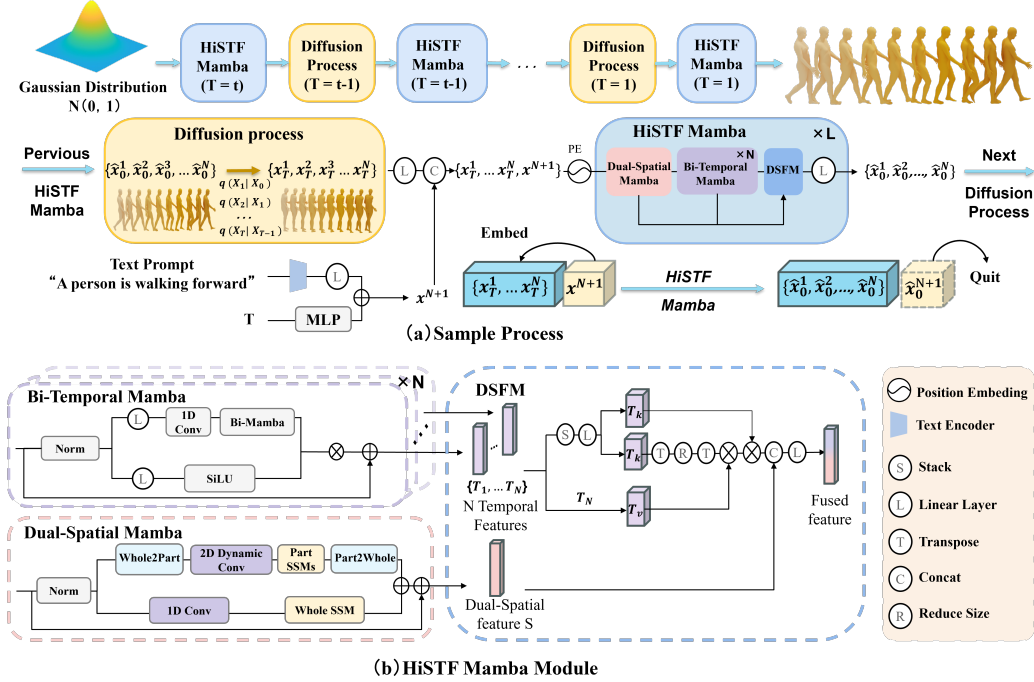


Figure 2: **The overview of the proposed HiSTF Mamba.** (a) **Sampling Process.** The model receives a text prompt as input and begins the iterative generation process from Gaussian noise, ultimately producing a noise-free action sequence x_0 that is semantically aligned with the prompt. (b) **HiSTF Mamba Module.** The HiSTF Mamba module primarily aims to predict a clean motion sequence $\{\hat{x}_0^1, \hat{x}_0^2, \dots, \hat{x}_0^N\}$ from a noisy input sequence $\{x_T^1, x_T^2, \dots, x_T^N\}$. By leveraging Bi-Temporal Mamba and Dual-Spatial Mamba, the model extracts temporal features $\{T_1, \dots, T_N\}$ and a spatial feature S . These N temporal features are then fed into the DSFM module to remove redundancy and are subsequently fused with S , producing a spatiotemporal motion representation that captures both joint-level details and overall body coordination. About Whole2Parts and Parts2Whole, see the appendix A.4

dimension $\mathbb{R}^{(B \times T \times D)}$. This bidirectional scanning strategy is particularly effective for modeling motion sequences. The forward branch captures how earlier actions influence and shape the current state, while the backward branch leverages future actions as contextual cues. By combining these two directions within a temporal recursion framework, the model more thoroughly encodes transitions and dependencies across time steps, ultimately producing more coordinated and smooth motion sequences.

Dual-Spatial Mamba. To address the limitation that existing spatial modules only focus on global motion features while neglecting fine-grained joint-level details, we propose the Dual-Spatial Mamba. This module performs two types of learning at the same time through Multi-Granular Body-Spatial Modelling, as described in Figure 2: on the Part-based the entire motion matrix is decomposed into 6 body part matrices, so that each input is limited to body part joints, allowing the model to focus on learning body part joint details, avoiding too much joint information being input at the same time, which can be severely compressed early on. The Whole-based retains the entire motion matrix inputs to learn whole-body motion coordination. Thus, Dual-Spatial Mamba adopts Part-based and Whole-based parallel learning to capture both local and global motion features, which are then fused via an element-wise addition strategy.

Specifically, the input sequence is normalized. In the Part-based learning phase, we first map the normalized full-body motion sequence back to its original dimensionality. Drawing upon insights from ParCo [57], we design a Whole2Part module to split the whole-body motion into six parts. R.Leg, L.Leg, Backbone, Root, R.Arm, and L.Arm. This design follows the common practice of 3D human body models (e.g., SMPL, MMM), where Kinematic Trees typically represent the skeleton as five main chains (the four limbs plus the backbone); We adds a separate Root component to account

for global trajectories, thereby leading to six sub-motions in total. Formally, given a motion sequence $x = \{x^1, x^2, x^3, \dots, x^N\}$, it is partitioned into $p_i = \{p_i^1, p_i^2, p_i^3, \dots, p_i^N\}$, $i \in \{1, 2, \dots, S\}$, where S denotes the total number of body parts. For more details about Whole2Parts and Parts2Whole, see the appendix A.4. After segmenting the motion into six parts, the features of each part are projected to a latent dimension and fed into a 2D dynamic convolution network. To better capture the distinct motion patterns of each part, six learnable convolution kernels are used, each corresponding to a specific body part, thus improving the model’s capability to capture fine-grained local details. Next, we stack the outputs of these six parts along the batch dimension and feed them into the Selected SSMs (Part Mamba) module, which further models local dependencies and outputs refined local motion features. Finally, through the Part2Whole process, we restore the local characteristics to a holistic representation of the entire body, thus obtaining fine-grained characteristics at the joint level. In Whole-based learning phase, the full-body motion matrix is fed into a 1D convolutional network to extract key motion features of different parts. Subsequently, by leveraging the Selected SSMs (Whole SSMs) module’s advantages in sequence processing and long-range dependency modeling, inter-joint relationships and latent motion patterns at the global level are captured, thereby yielding global motion features. Finally, Part-based and Whole-based motion features are summed element-wise to obtain a representation that combines both global motion patterns and fine-grained joint-level detail features.

3.4 Dynamic Spatiotemporal Fusion Module

To better integrate temporal and spatial features and enable the model to learn more expressive spatiotemporal representations, Inspired by the DMCA module in Sparx [58], we propose a dynamic spatiotemporal fusion module (DSFM). Differently, DSFM not only reduces redundancy and extracts complementary features among the output features from the N layers of Temporal Mamba, but also modifies the fusion strategy to effectively integrate this refined temporal features with spatial features to obtain an expressive spatiotemporal representation. Specifically, as shown in Fig. 2, let $Y \in \mathbb{R}^{(C \times T \times D)}$ represent the output features of N Temporal Mamba layers, where $Y = \{Y_1, Y_2, \dots, Y_N\}$. In practice, the output of Temporal Mamba is originally in the form $Y \in \mathbb{R}^{(T \times D)}$. To facilitate an effective division into Y_q and Y_k in the subsequent processing steps, we apply an unsqueeze operation to reshape it into $Y \in \mathbb{R}^{(C \times T \times D)}$. Additionally, let $S \in \mathbb{R}^{(T \times D)}$ denote the output features of Space Mamba. Here, C represents the number of channels, while T and D denote the sequence length and the feature dimension respectively.

To obtain refined temporal information, the first $N - 1$ temporal features $\{Y_1, Y_2, \dots, Y_{N-1}\}$ are stacked along the channel dimension and then projected into $\mathbb{R}^{(2C \times T \times D)}$. The projected features are subsequently split into two components, each squeezed to $\mathbb{R}^{(T \times D)}$. One component serves as the query Y_q , while the other serves as the key Y_k .

The attention matrix is computed using Y_v and Y_k . According to [58], this attention matrix is independent of the spatial dimension of Y_v and Y_k . Hence, a reduction by a factor of s can be applied, mapping Y_k, Y_v to $\mathbb{R}^{(T \times \frac{D}{s})}$. This step considerably lowers computational overhead and memory usage while preserving key temporal relationships. The resulting matrix is then used to weight the query Y_q , yielding the refined temporal feature.

Next, the refined temporal features are integrated with the spatial features. The resulting representations are concatenated along the feature dimension, forming $\mathbb{R}^{(T \times 2D)}$. Finally, a linear projection is applied to map the concatenated features back to $\mathbb{R}^{(T \times D)}$, ensuring a unified representation. This fusion mechanism allows the model to effectively capture complementary spatiotemporal patterns, enhancing its ability to learn robust feature representations.

Mathematically, the Dynamic Spatiotemporal Fusion Module (DSFM) can be formulated as follows:

$$\begin{aligned}
 Y_k, Y_q &= \text{squeeze}\left(\text{split}\left(W_1 \cdot \text{concat}(Y_1, Y_2, \dots, Y_{N-1})\right)\right), \\
 V &= R((Y_N)^T), \quad K = R((Y_k)^T), \quad Q = Y_q, \\
 \mathbf{T} &= \frac{\text{Softmax}(QK^T)}{\sqrt{N/r}} V, \quad Z = W_2 \cdot \text{Concat}(S, T).
 \end{aligned} \tag{3}$$

where W represents a linear projection. Specifically, $W_1 \in \mathbb{R}^{((N-1)C \times 2C)}$ performs a projection along the channel dimension, while $W_2 \in \mathbb{R}^{(2D \times D)}$ projects along the feature dimension. The function R denotes a reduction operation that decreases the feature dimension, implemented via a strided convolution. Additionally, $K, V \in \mathbb{R}^{(T \times \frac{D}{s})}$ represent the key and value matrices after dimensionality reduction.

4 Experiments

Methods	R Precision \uparrow			FID \downarrow	MM Dist \downarrow	Diversity \rightarrow	MModality \uparrow
	Top 1	Top 2	Top 3				
Real	0.511 \pm .003	0.703 \pm .003	0.797 \pm .002	0.002 \pm .000	2.974 \pm .008	9.503 \pm .065	-
T2M [28]	0.457 \pm .002	0.639 \pm .003	0.740 \pm .003	1.067 \pm .002	3.340 \pm .008	9.188 \pm .002	2.090 \pm .083
TEMOS [29]	0.424 \pm .002	0.612 \pm .002	0.722 \pm .002	3.734 \pm .028	3.703 \pm .008	8.973 \pm .071	0.368 \pm .018
MDM [18]	0.320 \pm .005	0.498 \pm .004	0.611 \pm .007	0.544 \pm .044	5.566 \pm .027	9.559 \pm .086	2.799 \pm .072
MotionDiffuse [20]	0.491 \pm .001	0.681 \pm .001	0.782 \pm .001	0.630 \pm .001	3.113 \pm .001	<u>9.410</u> \pm .049	1.553 \pm .042
MLD [19]	0.481 \pm .003	0.673 \pm .003	0.772 \pm .002	0.473 \pm .013	3.196 \pm .010	9.724 \pm .082	2.413 \pm .079
Fg-T2M [59]	0.492 \pm .002	0.683 \pm .003	0.783 \pm .002	<u>0.243</u> \pm .019	3.109 \pm .007	9.278 \pm .072	1.614 \pm .049
MMDM [60]	0.435 \pm .006	0.627 \pm .006	0.733 \pm .007	0.285 \pm .032	3.363 \pm .029	9.398 \pm .088	<u>2.701</u> \pm .083
Motion Mamba [24]	<u>0.502</u> \pm .003	<u>0.693</u> \pm .002	<u>0.792</u> \pm .002	0.281 \pm .009	<u>3.060</u> \pm .058	9.871 \pm .084	2.294 \pm .058
HiSTF Mamba (10-steps)	0.488 \pm .005	0.685 \pm .004	0.784 \pm .005	0.189 \pm .018	3.101 \pm .022	9.712 \pm .090	2.529 \pm .044
HiSTF Mamba (15-steps)	0.504 \pm .005	0.699 \pm .005	0.798 \pm .005	0.249 \pm .023	3.053 \pm .022	9.383 \pm .091	2.276 \pm .036

Table 1: Comparison of results on the HumanML3D test set. The right arrow (\rightarrow) indicates that values closer to real motions correspond to better performance. Each evaluation was run 20 times, and “ \pm ” denotes the 95% confidence interval. Bold text highlights the best scores, while underlined entries mark the second-best.

4.1 Datasets

To evaluate the effectiveness of our method, we conduct experiments on two widely-used text-to-motion datasets: HumanML3D [28] and KIT-ML [61]. HumanML3D consists of 14,616 motion sequences and 44,970 textual descriptions. Meanwhile, KIT-ML, introduced by Plappert et al., comprises 3,911 motion sequences and 6,278 natural language annotations. To ensure a fair comparison, we follow the evaluation protocol established in [28] for subsequent experiments.

4.2 Comparative Studies

We evaluated our method on the HumanML3D [28] and KIT-ML [61] datasets and compared it with several existing state-of-the-art approaches. Our method models motion data in a continuous representation, whereas existing VQ-VAE-based approaches discretize motion into tokens. Since each token typically corresponds to a short motion segment already present in the dataset, this discretization provides a natural advantage when computing the FID metric: the generated motions are more likely to resemble the real data distribution, resulting in better FID scores. In light of this, **we do not conduct a direct comparison with current VQ-VAE-based state-of-the-art methods** [36–38, 57, 62]. Specifically, we adopted the network structure described in Section 3.1, setting the number of model layers to $N = 3$ and $L = 2$. Meanwhile, to accelerate the sampling process, we employed DPM-Solver++ and selected $step = 10$ and $step = 15$ for inference. As shown in Tables 1 and 2, our method achieves significant performance improvements on both the HumanML3D and KIT-ML datasets. On HumanML3D, when $step = 10$ is used, our FID metric is further reduced from 0.281 (obtained by the state-of-the-art Motion Mamba) to 0.189, representing an improvement of more than 30%, and we also observe increased R-Precision and MultiModal Distance. On KIT-ML, our method similarly outperforms existing approaches in terms of R-Precision, FID, and MM Dist, with the MM Distance reduced to 2.819. Additionally, we present qualitative motion results in Fig. 3. Compared with other approaches, our method produces motions that more closely align with the text, exhibiting more detailed joint movements and better full-body coordination.

Methods	R Precision \uparrow			FID \downarrow	MM Dist \downarrow	Diversity \rightarrow	MModality \uparrow
	Top 1	Top 2	Top 3				
Real	0.424 \pm .005	0.649 \pm .006	0.779 \pm .006	0.031 \pm .004	2.788 \pm .012	11.08 \pm .097	-
T2M [28]	0.370 \pm .005	0.569 \pm .007	0.693 \pm .007	2.770 \pm .109	3.401 \pm .008	10.91 \pm .119	1.482 \pm .065
MDM [18]	0.164 \pm .004	0.291 \pm .004	0.396 \pm .004	0.497 \pm .021	9.191 \pm .022	10.85 \pm .109	1.907 \pm .214
MotionDiffuse [20]	0.417 \pm .004	0.621 \pm .004	0.739 \pm .004	1.954 \pm .062	2.958 \pm .005	11.10 \pm .143	0.730 \pm .013
MLD [19]	0.390 \pm .008	0.609 \pm .008	0.734 \pm .007	0.404 \pm .027	3.204 \pm .027	10.80 \pm .117	2.192 \pm .071
MMDM [60]	0.386 \pm .007	0.603 \pm .006	0.729 \pm .006	0.408 \pm .022	3.215 \pm .026	10.53 \pm .100	<u>2.261</u> \pm .144
Motion Mamba [24]	0.419 \pm .006	0.645 \pm .005	0.765 \pm .006	0.307 \pm .041	3.021 \pm .025	<u>11.02</u> \pm .098	1.678 \pm .064
HiSTF Mamba (10-steps)	<u>0.437</u> \pm .006	<u>0.651</u> \pm .006	<u>0.772</u> \pm .006	0.289 \pm .021	<u>2.846</u> \pm .018	10.92 \pm .096	1.512 \pm .088
HiSTF Mamba (15-steps)	0.440 \pm .006	0.657 \pm .006	0.774 \pm .006	<u>0.293</u> \pm .017	2.819 \pm .015	10.93 \pm .099	1.347 \pm .056

Table 2: Comparison of quantitative results on the KIT-ML dataset

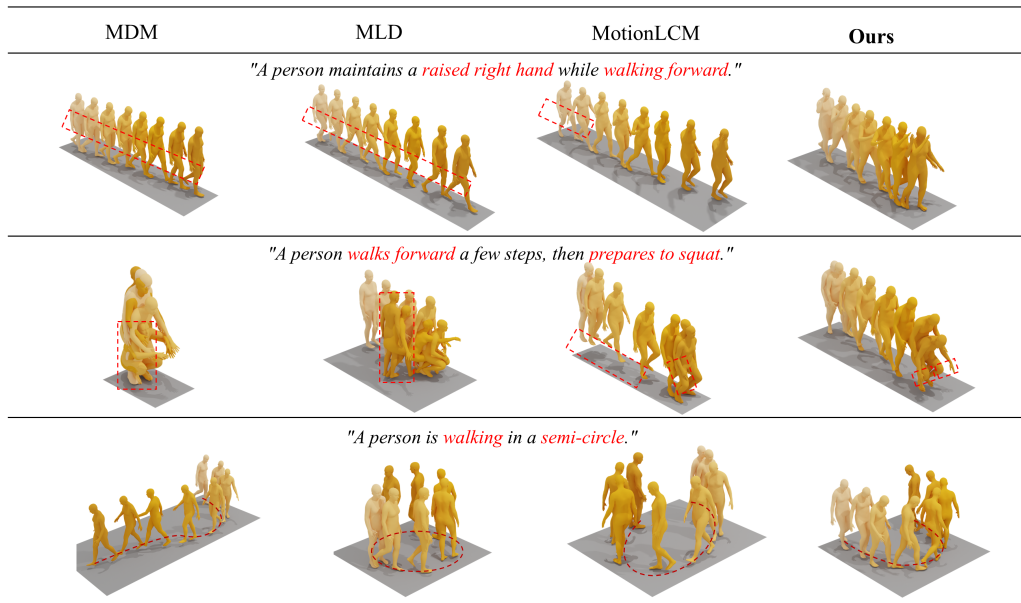


Figure 3: **Qualitative comparison of typical methods.** We randomly selected three textual samples to generate motion sequences. Our results exhibit closer alignment with the text and present richer joint-level details.

4.3 Ablation Studies

In this experiment, we investigate how the number of Bi-Temporal Mamba blocks (N), the total number of layers (L), and the presence or absence of key components DSFM, (whole-based learning, and part-based learning within Dual-Spatial Mamba’s two branches), as well as the entire Dual-Spatial Mamba and Bi-Temporal Mamba, affect the model’s performance on the HumanML3D dataset with an inference step of 10.

Ablation of layer. As shown in Table 3, we investigate how varying the number of Bi-Temporal Mamba blocks (N) and the total number of layers (L) impacts model performance. When configured with $N = 3$ and $L = 2$, our approach achieves the lowest Fréchet Inception Distance (FID) of 0.189, indicating a better capture of the underlying motion distribution. Although increasing N to 3 leads to gains in Multimodality, it also increases the parameter count and inference time, making $L = 2$ and $N = 3$ a favorable choice for balancing accuracy and computational cost.

Ablation of key components. Table 4 presents the ablation results for each key component. When ablating the entire Dual-Spatial Mamba and Bi-Temporal Mamba, we replace them with the same number of standard Transformer blocks for a fair comparison. Although this substitution slightly increases the number of parameters, it raises the FID to 0.367 and 0.439, indicating that removing these modules forfeits the ability to capture both global body coordination and fine-grained limb details. Moreover, ablating DSFM leads to a 207% increase in FID while saving 1.38M parameters,

N	L	R Precision \uparrow			FID \downarrow	MM Dist \downarrow	Diversity \rightarrow	MModality \uparrow	Parameters	AITS \downarrow
		Top 1	Top 2	Top 3						
	Real	0.511 \pm .003	0.703 \pm .003	0.797 \pm .002	0.002 \pm .000	2.974 \pm .008	9.503 \pm .065	-	-	-
2	2	0.484 \pm .007	0.679 \pm .006	0.780 \pm .006	0.358 \pm .033	3.132 \pm .016	9.693 \pm .083	2.530 \pm .063	11.90M	0.26s
3	2	0.488 \pm .005	0.685 \pm .004	0.784 \pm .005	0.189 \pm .018	3.101 \pm .022	9.712 \pm .090	2.529 \pm .044	15.53M	0.28s
4	2	0.487 \pm .006	0.675 \pm .005	0.773 \pm .005	0.409 \pm .036	3.223 \pm .031	9.938 \pm .066	2.622 \pm .035	19.17M	0.33s
2	3	0.469 \pm .005	0.666 \pm .006	0.767 \pm .006	0.490 \pm .036	3.242 \pm .024	10.060 \pm .010	2.619 \pm .078	17.32M	0.37s
3	3	0.471 \pm .005	0.665 \pm .005	0.767 \pm .005	0.339 \pm .036	3.241 \pm .023	9.783 \pm .095	2.721 \pm .056	22.77M	0.39s
4	3	0.471 \pm .007	0.667 \pm .008	0.763 \pm .007	0.337 \pm .040	3.298 \pm .031	9.831 \pm .085	2.780 \pm .078	28.22M	0.49s

Table 3: Ablation study on varying the number of Bi-Temporal Mamba blocks (N) and the total number of layers, evaluated on HumanML3D with an inference step of 10. AITS is the abbreviation of average inference time per sentence. Parameters refers to the total number of model parameters.

demonstrating that DSFM is effective spatiotemporal fusion with acceptable parameter cost. We also examine the roles of Whole-based and Part-based branches in Dual-Spatial Mamba. Removing the Part-based branch lowers the AITS to 0.18s, showing that the additional latency primarily arises from large matrix operations rather than increased parameter count. Nevertheless, the Part-based branch indeed improves performance, underscoring its effectiveness. These findings confirm the effectiveness of all proposed components in capturing both fine-grained joint details and overall body coordination, thereby enhancing the quality and accuracy of text-to-motion generation.

BTM	Whole-b	Part-b	DSFM	R Precision \uparrow			FID \downarrow	MM Dist \downarrow	Diversity \rightarrow	MModality \uparrow	Parameters	AITS \downarrow
				Top 1	Top 2	Top 3						
		Real		0.511 \pm .003	0.703 \pm .003	0.797 \pm .002	0.002 \pm .000	2.974 \pm .008	9.503 \pm .065	-	-	-
\checkmark		\checkmark	\checkmark	0.482 \pm .007	0.678 \pm .006	0.772 \pm .005	0.368 \pm .033	3.747 \pm .029	9.933 \pm .059	2.601 \pm .078	14.99M	0.25s
\checkmark	\checkmark	\checkmark	\checkmark	0.482 \pm .006	0.677 \pm .006	0.779 \pm .005	0.303 \pm .026	3.177 \pm .019	9.988 \pm .092	2.440 \pm .067	14.43M	0.18s
\checkmark		\checkmark	\checkmark	0.473 \pm .006	0.664 \pm .007	0.764 \pm .004	0.367 \pm .035	3.269 \pm .244	9.847 \pm .102	2.510 \pm .104	19.65M	0.21s
	\checkmark	\checkmark	\checkmark	0.478 \pm .006	0.672 \pm .007	0.771 \pm .005	0.439 \pm .035	3.206 \pm .019	9.817 \pm .094	2.536 \pm .079	23.55M	0.23s
\checkmark	\checkmark	\checkmark	\checkmark	0.464 \pm .006	0.661 \pm .007	0.764 \pm .004	0.581 \pm .054	3.198 \pm .022	9.359 \pm .099	2.590 \pm .079	14.15M	0.25s
\checkmark	\checkmark	\checkmark	\checkmark	0.488 \pm .005	0.685 \pm .004	0.784 \pm .005	0.189 \pm .018	3.101 \pm .022	9.712 \pm .090	2.529 \pm .044	15.53M	0.28s

Table 4: Ablation study on key components, evaluated on HumanML3D with an inference step of 10. For simplicity, we use **BTM** to represent *Bi-Temporal Mamba*, and **Part-b** and **Whole-b** to denote the part-based learning and whole-based learning in *Dual-Spatial Mamba*, respectively.

4.4 Implementation Details

All models in the HiSTF Mamba use the AdamW optimizer, with the learning rate maintained at 1×10^{-4} . The average training step is about 570k, and we set the batch size to 64. We fix the diffusion step count at 1000 and use 10 or 15 sampling steps. On a single NVIDIA GEFORCE RTX 4090 GPU, training on the HumanML3D dataset takes approximately 37.5 hours. The average inference time is about 0.28 seconds, and our model has a total parameter count of 15.53M. Further details on both inference time and total parameters can be found in the appendix A.1.

5 Conclusion

We introduced **HiSTF Mamba**, a text-to-motion generation framework that combines local and global spatial features with bidirectional temporal modeling. Its *Dual-Spatial Mamba* block captures both fine-grained joint dynamics and coarse whole-body movements, while the *Bi-Temporal Mamba* block encodes short-term and long-term dependencies in a bidirectional manner. To fuse refined temporal features with spatial representations, we proposed the *DSFM* block, which reduces redundancy and boosts overall spatiotemporal expressiveness.

Although our model still has many limitations (appendix A.5), extensive experiments on HumanML3D and KIT-ML confirm that **HiSTF Mamba** achieves robust performance across multiple evaluation metrics, while producing high-fidelity and semantically aligned motion sequences. Our method achieves these results with efficient training and rapid inference. We believe **HiSTF Mamba** provides a promising avenue for generating realistic, detail-rich human motions, and it can serve as a foundation for future text-to-motion research.

References

- [1] Jehee Lee, Jinxiang Chai, Paul SA Reitsma, Jessica K Hodgins, and Nancy S Pollard. Interactive control of avatars animated with human motion data. In *Proceedings of the 29th annual conference on Computer graphics and interactive techniques*, pages 491–500, 2002.
- [2] Moritz Kappel, Vladislav Golyanik, Mohamed Elgharib, Jann-Ole Henningson, Hans-Peter Seidel, Susana Castillo, Christian Theobalt, and Marcus Magnor. High-fidelity neural human motion transfer from monocular video. In *Proceedings of the IEEE/CVF conference on computer vision and pattern recognition*, pages 1541–1550, 2021.
- [3] Hema S Koppula and Ashutosh Saxena. Anticipating human activities using object affordances for reactive robotic response. *IEEE transactions on pattern analysis and machine intelligence*, 38(1):14–29, 2015.
- [4] Ian Goodfellow, Jean Pouget-Abadie, Mehdi Mirza, Bing Xu, David Warde-Farley, Sherjil Ozair, Aaron Courville, and Yoshua Bengio. Generative adversarial networks. *Communications of the ACM*, 63(11): 139–144, 2020.
- [5] Diederik P Kingma, Max Welling, et al. Auto-encoding variational bayes. 2013.
- [6] Jogendra Nath Kundu, Maharshi Gor, and R Venkatesh Babu. Bihmp-gan: Bidirectional 3d human motion prediction gan. In *Proceedings of the AAAI conference on artificial intelligence*, volume 33, pages 8553–8560, 2019.
- [7] Liang Xu, Ziyang Song, Dongliang Wang, Jing Su, Zhicheng Fang, Chenjing Ding, Weihao Gan, Yichao Yan, Xin Jin, Xiaokang Yang, et al. Actformer: A gan-based transformer towards general action-conditioned 3d human motion generation. In *Proceedings of the IEEE/CVF International Conference on Computer Vision*, pages 2228–2238, 2023.
- [8] Qiongjie Cui, Huaijiang Sun, Yue Kong, Xiaoqian Zhang, and Yanmeng Li. Efficient human motion prediction using temporal convolutional generative adversarial network. *Information Sciences*, 545: 427–447, 2021.
- [9] Deepak Kumar Jain, Masoumeh Zareapoor, Rachna Jain, Abhishek Kathuria, and Shivam Bachhety. Gan-pose: an improvised bidirectional gan model for human motion prediction. *Neural Computing and Applications*, 32(18):14579–14591, 2020.
- [10] Emad Barsoum, John Kender, and Zicheng Liu. Hp-gan: Probabilistic 3d human motion prediction via gan. In *Proceedings of the IEEE conference on computer vision and pattern recognition workshops*, pages 1418–1427, 2018.
- [11] Avinash Amballa, Gayathri Akkinapalli, and Vinitra Muralikrishnan. Ls-gan: Human motion synthesis with latent-space gans. *arXiv preprint arXiv:2501.01449*, 2024.
- [12] Xiaoyu Bie, Wen Guo, Simon Leglaive, Lauren Girin, Francesc Moreno-Noguer, and Xavier Alameda-Pineda. Hit-dvae: Human motion generation via hierarchical transformer dynamical vae. *arXiv preprint arXiv:2204.01565*, 2022.
- [13] Taku Komura, Ikhsanul Habibie, Daniel Holden, Jonathan Schwarz, and Joe Yearsley. A recurrent variational autoencoder for human motion synthesis. In *The 28th British Machine Vision Conference*, 2017.
- [14] Xinchun Yan, Akash Rastogi, Ruben Villegas, Kalyan Sunkavalli, Eli Shechtman, Sunil Hadap, Ersin Yumer, and Honglak Lee. Mt-vae: Learning motion transformations to generate multimodal human dynamics. In *Proceedings of the European conference on computer vision (ECCV)*, pages 265–281, 2018.
- [15] Yuichiro Motegi, Yuma Hijioka, and Makoto Murakami. Human motion generative model using variational autoencoder. *Int J Model Optim*, 8(1):8–12, 2018.
- [16] Anindita Ghosh, Noshaba Cheema, Cennet Oguz, Christian Theobalt, and Philipp Slusallek. Synthesis of compositional animations from textual descriptions. In *Proceedings of the IEEE/CVF international conference on computer vision*, pages 1396–1406, 2021.
- [17] Jonathan Ho, Ajay Jain, and Pieter Abbeel. Denoising diffusion probabilistic models. volume 33, pages 6840–6851, 2020.
- [18] Guy Tevet, Sigal Raab, Brian Gordon, Yonatan Shafir, Daniel Cohen-Or, and Amit H Bermano. Human motion diffusion model. 2022.

- [19] Xin Chen, Biao Jiang, Wen Liu, Zilong Huang, Bin Fu, Tao Chen, and Gang Yu. Executing your commands via motion diffusion in latent space. In *Proceedings of the IEEE/CVF conference on computer vision and pattern recognition*, pages 18000–18010, 2023.
- [20] Mingyuan Zhang, Zhongang Cai, Liang Pan, Fangzhou Hong, Xinying Guo, Lei Yang, and Ziwei Liu. Motiondiffuse: Text-driven human motion generation with diffusion model. *IEEE transactions on pattern analysis and machine intelligence*, 46(6):4115–4128, 2024.
- [21] Rishabh Dabral, Muhammad Hamza Mughal, Vladislav Golyanik, and Christian Theobalt. Mofusion: A framework for denoising-diffusion-based motion synthesis. In *Proceedings of the IEEE/CVF conference on computer vision and pattern recognition*, pages 9760–9770, 2023.
- [22] Mingyuan Zhang, Huirong Li, Zhongang Cai, Jiawei Ren, Lei Yang, and Ziwei Liu. Finemogen: Fine-grained spatio-temporal motion generation and editing. *Advances in Neural Information Processing Systems*, 36:13981–13992, 2023.
- [23] Chang Liu, Mengyi Zhao, Bin Ren, Mengyuan Liu, Nicu Sebe, et al. Spatio-temporal graph diffusion for text-driven human motion generation. In *BMVC*, pages 722–729, 2023.
- [24] Zeyu Zhang, Akide Liu, Ian Reid, Richard Hartley, Bohan Zhuang, and Hao Tang. Motion mamba: Efficient and long sequence motion generation. In *European Conference on Computer Vision*, pages 265–282. Springer, 2024.
- [25] Albert Gu and Tri Dao. Mamba: Linear-time sequence modeling with selective state spaces. *arXiv preprint arXiv:2312.00752*, 2023.
- [26] Hyemin Ahn, Timothy Ha, Yunho Choi, Hwiyeon Yoo, and Songhwai Oh. Text2action: Generative adversarial synthesis from language to action. In *2018 IEEE International Conference on Robotics and Automation (ICRA)*, pages 5915–5920. IEEE, 2018.
- [27] Chaitanya Ahuja and Louis-Philippe Morency. Language2pose: Natural language grounded pose forecasting. In *2019 International conference on 3D vision (3DV)*, pages 719–728. IEEE, 2019.
- [28] Chuan Guo, Shihao Zou, Xinxin Zuo, Sen Wang, Wei Ji, Xingyu Li, and Li Cheng. Generating diverse and natural 3d human motions from text. In *Proceedings of the IEEE/CVF conference on computer vision and pattern recognition*, pages 5152–5161, 2022.
- [29] Mathis Petrovich, Michael J Black, and Gül Varol. Temos: Generating diverse human motions from textual descriptions. In *European Conference on Computer Vision*, pages 480–497. Springer, 2022.
- [30] Nikos Athanasiou, Mathis Petrovich, Michael J Black, and Gül Varol. Teach: Temporal action composition for 3d humans. In *2022 International Conference on 3D Vision (3DV)*, pages 414–423. IEEE, 2022.
- [31] Guy Tevet, Brian Gordon, Amir Hertz, Amit H Bermano, and Daniel Cohen-Or. Motionclip: Exposing human motion generation to clip space. In *European Conference on Computer Vision*, pages 358–374. Springer, 2022.
- [32] Alec Radford, Jong Wook Kim, Chris Hallacy, Aditya Ramesh, Gabriel Goh, Sandhini Agarwal, Girish Sastry, Amanda Askell, Pamela Mishkin, Jack Clark, et al. Learning transferable visual models from natural language supervision. In *International conference on machine learning*, pages 8748–8763. PmLR, 2021.
- [33] Chuan Guo, Xinxin Zuo, Sen Wang, and Li Cheng. Tm2t: Stochastic and tokenized modeling for the reciprocal generation of 3d human motions and texts. In *European Conference on Computer Vision*, pages 580–597. Springer, 2022.
- [34] Aaron Van Den Oord, Oriol Vinyals, et al. Neural discrete representation learning. *Advances in neural information processing systems*, 30, 2017.
- [35] Jianrong Zhang, Yangsong Zhang, Xiaodong Cun, Yong Zhang, Hongwei Zhao, Hongtao Lu, Xi Shen, and Ying Shan. Generating human motion from textual descriptions with discrete representations. In *Proceedings of the IEEE/CVF conference on computer vision and pattern recognition*, pages 14730–14740, 2023.
- [36] Ekkasit Pinyoanuntapong, Pu Wang, Minwoo Lee, and Chen Chen. Mmm: Generative masked motion model. In *Proceedings of the IEEE/CVF Conference on Computer Vision and Pattern Recognition*, pages 1546–1555, 2024.

- [37] Chuan Guo, Yuxuan Mu, Muhammad Gohar Javed, Sen Wang, and Li Cheng. Momask: Generative masked modeling of 3d human motions. In *Proceedings of the IEEE/CVF Conference on Computer Vision and Pattern Recognition*, pages 1900–1910, 2024.
- [38] Ekkasit Pinyoanuntapong, Muhammad Usama Saleem, Pu Wang, Minwoo Lee, Srijan Das, and Chen Chen. Bamm: bidirectional autoregressive motion model. In *European Conference on Computer Vision*, pages 172–190. Springer, 2024.
- [39] Wenxun Dai, Ling-Hao Chen, Jingbo Wang, Jinpeng Liu, Bo Dai, and Yansong Tang. Motionlcm: Real-time controllable motion generation via latent consistency model. In *European Conference on Computer Vision*, pages 390–408. Springer, 2024.
- [40] Simian Luo, Yiqin Tan, Longbo Huang, Jian Li, and Hang Zhao. Latent consistency models: Synthesizing high-resolution images with few-step inference. *arXiv preprint arXiv:2310.04378*, 2023.
- [41] Wenyang Zhou, Zhiyang Dou, Zeyu Cao, Zhouyingcheng Liao, Jingbo Wang, Wenjia Wang, Yuan Liu, Taku Komura, Wenping Wang, and Lingjie Liu. Emdm: Efficient motion diffusion model for fast and high-quality motion generation. In *European Conference on Computer Vision*, pages 18–38. Springer, 2024.
- [42] Ashish Vaswani, Noam Shazeer, Niki Parmar, Jakob Uszkoreit, Llion Jones, Aidan N Gomez, Łukasz Kaiser, and Illia Polosukhin. Attention is all you need. *Advances in neural information processing systems*, 30, 2017.
- [43] Albert Gu, Karan Goel, and Christopher Ré. Efficiently modeling long sequences with structured state spaces. *arXiv preprint arXiv:2111.00396*, 2021.
- [44] Albert Gu, Isys Johnson, Karan Goel, Khaled Saab, Tri Dao, Atri Rudra, and Christopher Ré. Combining recurrent, convolutional, and continuous-time models with linear state space layers. *Advances in neural information processing systems*, 34:572–585, 2021.
- [45] Albert Gu, Tri Dao, Stefano Ermon, Atri Rudra, and Christopher Ré. Hippo: Recurrent memory with optimal polynomial projections. *Advances in neural information processing systems*, 33:1474–1487, 2020.
- [46] Lianghui Zhu, Bencheng Liao, Qian Zhang, Xinlong Wang, Wenyu Liu, and Xinggang Wang. Vision mamba: Efficient visual representation learning with bidirectional state space model. In *Forty-first International Conference on Machine Learning*, 2024.
- [47] Yue Liu, Yunjie Tian, Yuzhong Zhao, Hongtian Yu, Lingxi Xie, Yaowei Wang, Qixiang Ye, Jianbin Jiao, and Yunfan Liu. Vmamba: Visual state space model. *Advances in neural information processing systems*, 37:103031–103063, 2025.
- [48] Chenhongyi Yang, Zehui Chen, Miguel Espinosa, Linus Ericsson, Zhenyu Wang, Jiaming Liu, and Elliot J Crowley. Plainmamba: Improving non-hierarchical mamba in visual recognition. *arXiv preprint arXiv:2403.17695*, 2024.
- [49] Tao Huang, Xiaohuan Pei, Shan You, Fei Wang, Chen Qian, and Chang Xu. Localmamba: Visual state space model with windowed selective scan. *arXiv preprint arXiv:2403.09338*, 2024.
- [50] Xiaohuan Pei, Tao Huang, and Chang Xu. Efficientvmamba: Atrous selective scan for light weight visual mamba. *arXiv preprint arXiv:2403.09977*, 2024.
- [51] Chi-Sheng Chen, Guan-Ying Chen, Dong Zhou, Di Jiang, and Dai-Shi Chen. Res-vmamba: Fine-grained food category visual classification using selective state space models with deep residual learning. *arXiv preprint arXiv:2402.15761*, 2024.
- [52] Hang Guo, Jinmin Li, Tao Dai, Zhihao Ouyang, Xudong Ren, and Shu-Tao Xia. Mambair: A simple baseline for image restoration with state-space model. In *European conference on computer vision*, pages 222–241. Springer, 2024.
- [53] Zhen Zou, Hu Yu, Jie Huang, and Feng Zhao. Freqmamba: Viewing mamba from a frequency perspective for image deraining. In *Proceedings of the 32nd ACM International Conference on Multimedia*, pages 1905–1914, 2024.
- [54] Wenrui Li, Xiaopeng Hong, Ruiqin Xiong, and Xiaopeng Fan. Spikemba: Multi-modal spiking saliency mamba for temporal video grounding. *arXiv preprint arXiv:2404.01174*, 2024.
- [55] Kunchang Li, Xinhao Li, Yi Wang, Yinan He, Yali Wang, Limin Wang, and Yu Qiao. Videomamba: State space model for efficient video understanding. In *European Conference on Computer Vision*, pages 237–255. Springer, 2024.

- [56] Cheng Lu, Yuhao Zhou, Fan Bao, Jianfei Chen, Chongxuan Li, and Jun Zhu. Dpm-solver: A fast ode solver for diffusion probabilistic model sampling in around 10 steps. *Advances in Neural Information Processing Systems*, 35:5775–5787, 2022.
- [57] Qiran Zou, Shangyuan Yuan, Shian Du, Yu Wang, Chang Liu, Yi Xu, Jie Chen, and Xiangyang Ji. Parco: Part-coordinating text-to-motion synthesis. In *European Conference on Computer Vision*, pages 126–143. Springer, 2024.
- [58] Meng Lou, Yunxiang Fu, and Yizhou Yu. Sparx: A sparse cross-layer connection mechanism for hierarchical vision mamba and transformer networks. *arXiv preprint arXiv:2409.09649*, 2024.
- [59] Yin Wang, Zhiying Leng, Frederick WB Li, Shun-Cheng Wu, and Xiaohui Liang. Fg-t2m: Fine-grained text-driven human motion generation via diffusion model. In *Proceedings of the IEEE/CVF International Conference on Computer Vision*, pages 22035–22044, 2023.
- [60] Xingyu Chen. Text-driven human motion generation with motion masked diffusion model. *arXiv preprint arXiv:2409.19686*, 2024.
- [61] Matthias Plappert, Christian Mandery, and Tamim Asfour. The kit motion-language dataset. *Big data*, 4(4): 236–252, 2016.
- [62] Biao Jiang, Xin Chen, Wen Liu, Jingyi Yu, Gang Yu, and Tao Chen. Motiongpt: Human motion as a foreign language. *Advances in Neural Information Processing Systems*, 36:20067–20079, 2023.

A Technical Appendices and Supplementary Material

A.1 Inference Time and Total Parameters

To compute the Average Inference Time per Sentence (AITS), we follow the procedure in [19] and report AITS in seconds. We measure AITS on the HumanML3D test set [28] with a batch size of 1, excluding any overhead for model and dataset loading. As shown in Fig. 4, our method requires **0.280 s** per sentence, which is slower than TEMOS [29] and Motion Mamba [24]. However, this additional runtime yields marked performance gains: our approach reduces the FID to **0.189**, outperforming all other methods in the figure. Although our model introduces more complexity at first glance, it maintains a parameter count of just **15.53 M**, around **13%** fewer than the baseline MDM [60] (17.88 M). In short, our model’s acceptable increase in inference time and complexity yields a improvement in generation quality.

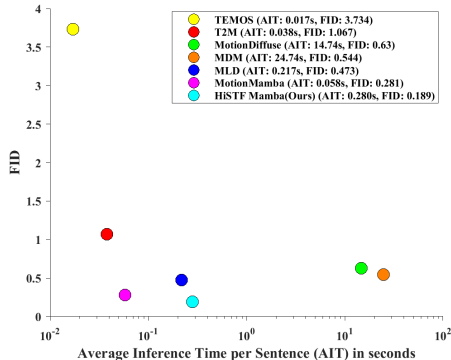


Figure 4: Comparison of HiSTF Mamba’s AITS and FID with other baseline methods.

A.2 Loss of HiSTF Mamba

Let x_0 be the ground-truth motion sequence, \hat{x}_0 the predicted motion, and c the textual condition. We denote $FK(\cdot)$ as the forward kinematics function, which converts joint rotations into 3D coordinates (or the identity if positions are already provided). The term N indicates the total number of frames in the motion, and f_i is the binary mask for foot contact at frame i , where $f_i \in \{0, 1\}$ and is applied only to foot joints in the sequence.

The primary training loss function of HiSTF Mamba is defined as $\mathcal{L}_{\text{simple}}$, where in HiSTF Mamba we predict the simple objective directly, i.e., $\hat{x}_0 = f(x_t, t, c)$. the primary loss is defined as:

$$\mathcal{L}_{\text{simple}} = \mathbb{E}_{x_0 \sim q(x_0|c), t \sim [1, T]} \left[\|x_0 - f(x_t, t, c)\| \right]. \tag{4}$$

In addition, we incorporate the position loss, foot contact loss, and velocity loss to encourage physically plausible motions:

$$\mathcal{L}_{\text{pos}} = \frac{1}{N} \sum_{i=1}^N \|FK(x_0^i) - FK(\hat{x}_0^i)\|_2^2, \tag{5}$$

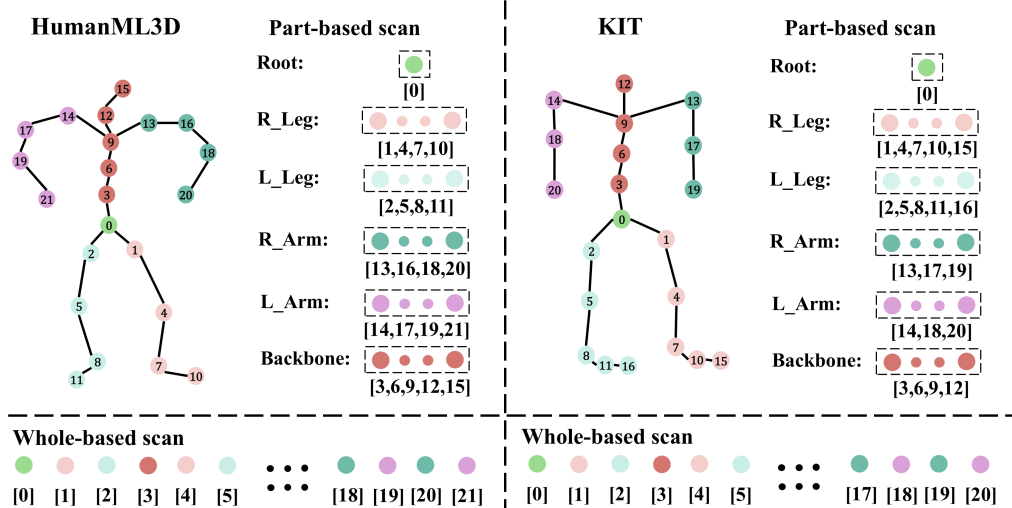


Figure 5: Illustration of the part-based and whole-based skeletal scans on the HumanML3D [28] (left) and KIT [61] (right) datasets.

$$\mathcal{L}_{\text{foot}} = \frac{1}{N-1} \sum_{i=1}^{N-1} \left\| (FK(x_0^{i+1}) - FK(x_0^i)) \cdot f_i \right\|_2^2, \quad (6)$$

$$\mathcal{L}_{\text{vel}} = \frac{1}{N-1} \sum_{i=1}^{N-1} \left\| ((x_0^{i+1} - x_0^i) - (\hat{x}_0^{i+1} - \hat{x}_0^i)) \right\|_2^2. \quad (7)$$

Thus, the total loss is formulated as:

$$\mathcal{L} = \mathcal{L}_{\text{simple}} + \lambda_{\text{pos}} \mathcal{L}_{\text{pos}} + \lambda_{\text{vel}} \mathcal{L}_{\text{vel}} + \lambda_{\text{foot}} \mathcal{L}_{\text{foot}}. \quad (8)$$

A.3 Evaluation Metrics

In this work, we employ the method described in [28] to evaluate our approach, using five evaluation metrics. including (1) **Fréchet Inception Distance (FID)**, which serves as the primary metric to assess the difference in feature distributions between generated motions and real motions; (2) **R-Precision** evaluates how well a generated motion aligns with its corresponding textual description. It measures the retrieval accuracy by checking whether the ground truth description ranks among the top-k closest matches based on Euclidean distances between motion and text features; (3) **MultiModal Distance (MM Dist)**, which calculates the average distance between generated motions and their corresponding text descriptions; (4) **Diversity** measures the variety of generated motions and is computed as the variance of motion features; (5) **Multimodality** evaluates the variety of motions generated from the same text description.

A.4 Details of Whole2Part and Part2Whole

As illustrated in Fig 5, both HumanML3D [28] and KIT [61] skeletons are each divided into six body segments: Root, R_Leg, L_Leg, Backbone, R_Arm, and L_Arm. Each circle represents a specific joint index. Under the *part-based scan*, joints belonging to the same body segment are grouped together, enabling fine-grained modeling of local kinematic relationships. In contrast, the *whole-based scan* processes the entire skeleton as a single sequence of joint indices. By integrating both strategies, our Dual-Spatial Mamba simultaneously captures detailed joint-level nuances and preserves global body coordination.

A.5 Limitations

(1) Matrix operations in part-based learning: Our Dual-Spatial Mamba adopts a Whole2Part and Part2Whole scheme, which involves extensive matrix operations. Specifically, we split the full-body matrix into six distinct body-part matrices and then merge them back. Because the model must continuously learn both fine-grained joint dynamics and overall body coordination, these operations cannot be preprocessed and must be incorporated into the training process, thereby increasing the inference time.

(2) Performance compared to VQ-VAE-based methods: Although our method achieves noticeable performance gains, some evaluation metrics still fall short when compared to state-of-the-art approaches [36–38, 57, 62] using VQ-VAE.